Advances in Water Resources 34 (2011) 1049–1058

Contents lists available at ScienceDirect

Advances in Water Resources

journal homepage: www.elsevier.com/locate/advwatres

Unsteady overland flow on flat surfaces induced by spatial permeability contrasts

Sally Thompson [a,*], Gabriel Katul [a,b], Alexandra Konings [a], Luca Ridolfi [b]

[a] Nicholas School of the Environment, Duke University, Durham, NC 27707, USA
[b] Dipartimento di Idraulica, Trasporti e Infrastrutture Civili, Politecnico di Torino, C.so Duca degli Abruzzi, 24, 10129 Torino, Italy

ARTICLE INFO

Article history:
Received 9 February 2011
Received in revised form 30 May 2011
Accepted 31 May 2011
Available online 12 June 2011

Keywords:
Arid ecosystems
Hydraulics
Infiltration
Manning's equation
Overland flow
Patchy vegetation

ABSTRACT

Lateral redistribution of surface water in patchy arid ecosystems has been hypothesized to contribute to the maintenance of vegetation patches through the provision of a water subsidy from bare sites to vegetated sites. Such runon–runoff processes occur during Hortonian runoff events on topographically sloping ground. Surface flow redistribution may also occur on topographically flat ground if the presence of the vegetation patch creates a contrast in infiltration rate, leading to a free-surface gradient in ponded water. The precise dynamics and the eco-hydrologic role of this process has resisted complete theoretical treatment to date. Here the overland flow equations are modified to account for the presence of vegetation situated over a flat surface. The resulting model is solved numerically to determine whether this mechanism could influence the spatial partitioning of water in patchy arid ecosystems. Assumptions made about infiltration processes and overland flow in existing eco-hydrologic models of patchy and patterned arid ecosystems are evaluated in comparison to the solution of the 'full' coupled Saint–Venant equations with various infiltration models. The results indicate that the optimization of vegetation spatial patch scales with respect to water redistribution may be determined by the size of the infiltration redistribution length L over which the presence of an infiltration contrast perturbs baseline infiltration behavior.

1. Introduction

The lateral redistribution of ponded water generated during intense rainstorms plays an important role in the hydrological, biogeochemical and ecological functioning of patchy arid ecosystems. For instance, it is broadly accepted that the maintenance of vegetation in patchy arid systems is supported by lateral subsidies of rainfall from bare sites to vegetated ones [1–4]. However, the relative importance of above ground and below ground (via root uptake) water redistribution processes remains unresolved, particularly on flat sites [5–8]. At those flat sites, one working hypothesis is that the combined infiltration contrast and the efficiency of surface lateral transport alone can generate sufficient subsidies of water from bare sites to satisfy water demand in vegetated patches [6–8].

The potential energy gradients that drive overland flow can arise either from the topographic slope of the soil surface, or, in the absence of slope, from gradients in the free water surface. The former situation is typically assumed in hydrological routing models, and presumes that on flat terrain hydrological routing collapses to a simple one dimensional infiltration problem [9–11]. Redistribution of water in response to a free-surface gradient in the absence of a topographic slope, however, is known to be important in engineering applications such as irrigation or dam-removal [12,13]. On flat ground, which occurs in several areas with vegetation patterning [8], similar gradients could hypothetically arise during Hortonian runoff generation if a pronounced spatial contrast in rainfall intensity or infiltration rate create contrasting depths in ponded head through space. These mechanisms persist in the presence of a ground slope but become less important for sustaining lateral flow as the ground slope becomes large compared to the free surface gradients.

The pronounced contrasts in infiltration rate needed to generate this free-surface contrast can arise in patchily-vegetated arid ecosystems. In many such ecosystems, different soil surface conditions are found in vegetated and bare sites. These differences can result in 10-fold differences in infiltration capacity over relatively short distances (a few meters) [14,15]. Both physical and biological processes are involved in sustaining these differences. Enhanced biological activity in vegetated sites leads to increased soil macroporosity, often in association with termite activity [16–18]. The presence of the plant canopy and litter layer protect the soil surface from rain splash impacts and prevent the formation of photosynthetic biological soil crusts [19]. By comparison, bare sites are frequently colonized by crust-forming biota, and form physical soil crusts and seals in response to rain splash impact [20–22]. Although individual plants may be associated with shallow mound formation, these mounds are also associated with enhanced infiltration capacities. The proposed redistribution mechanism can still apply, although the routing would need to be amended to account for the microtopographic geometry [23].

* Corresponding author.
E-mail address: set8@duke.edu (S. Thompson).

0309-1708/$ - see front matter © 2011 Elsevier Ltd. All rights reserved.
doi:10.1016/j.advwatres.2011.05.012

The lateral fluxes of water that arise from the contrasts in ponded depth are a function of the water depth h, its spatial gradients $\partial h/\partial x$, and the hydrodynamic roughness of the ground surface. In patchily vegetated sites, the spatial contrasts in vegetation also lead to a contrast in hydrodynamic roughness, which tends to oppose the flow [24]. Thus the lateral redistribution of rainfall from bare sites to vegetated sites arises from a dynamic interplay of hydrological (infiltration contrasts) and hydraulic (roughness contrasts) processes.

The spatial dynamics of vegetation and their link to water availability in patchy ecosystems with low slopes have been addressed theoretically by several investigators using partial-differential-equation based models of coupled biomass-water movement [6,8,25,26]. Such simple models reproduce the observed morphology of patchy vegetation in arid ecosystems. To date, no model has explicitly confronted a mechanistic description of the unsteady hydraulic and hydrological aspects of the flow problems, but have instead made two simplifying assumptions:

1. The infiltration rate (f_c) could be represented as being linearly dependent upon the depth of ponded water (h); and
2. The overland flow (q) in an arbitrary direction x linearly scales with $\partial h/\partial x$.

The first of these assumptions, although non-standard compared to conventional infiltration theory, gains support from the role of microtopographic variability and macroporosity in infiltration dynamics. For instance, Dunne et al. [27] showed that where point-scale infiltration capacity was correlated with elevation along microtopographic profiles, bulk infiltration rates depended on the depth of inundation. Fox et al. [28] demonstrated an apparent depth dependence on infiltration capacity arising due to similar mechanisms in crusted soils. Novak et al. [29] similarly showed that the effects of crack structures on infiltration dynamics could be parameterized by treating the infiltration flux as depth-dependent. Both microtopographic variation and macroporosity are likely to arise in vegetated sites, and this h-dependent infiltration representation may be reasonable in a first-order analysis. The second assumption, however, removes the flow-depth nonlinearities arising from the shallow-water equations. Its use is primarily based on mathematical tractability rather than physical reasoning.

Existing theoretical models suggest that redistribution of water in response to the infiltration contrast on flat terrain may be sufficient to sustain the patchy characteristics of arid ecosystems [6,8]. However, it is unclear whether these results are biased by the assumptions made about infiltration and hydraulics described above. The goal of this work is to assess whether the lateral redistribution of water induced by the infiltration contrast can generate sufficiently large fluxes of water to meet water demand in these systems. The study is facilitated by two recent theoretical developments. The first is a novel representation of flow resistance associated with vegetation canopy density (presented below), and the second is a meta-analysis linking above-ground vegetation biomass to the enhancement of infiltration capacity in xeric sites [14]. These results are incorporated into a parameterization of the Saint–Venant equations, and are used to explore the redistribution of water from bare to vegetated sites as driven by variable infiltration rates. This exploration is organized around two key research questions:

1. Can contrasts in infiltration rate and surface roughness lead to a lateral redistribution of water from bare to vegetated sites? How large is this redistribution, over what spatial scales does it act, and how sensitive is it to soil, vegetation and storm properties? and
2. How sensitive are the predictions about the lateral redistribution to the assumptions made about infiltration, roughness, and to the choice of hydraulic model used to parameterize the flow?

The theoretical description of the problem is developed first, followed by a report on numerical investigations aimed at addressing these research questions.

2. Theory

The basic flow equations describing this problem are the Saint–Venant equations, modified to account for the influence of vegetation. The Saint–Venant equations are widely used to describe shallow overland flows, for which the assumptions that underpin their derivation, namely that the flow is nearly one-dimensional and that the momentum equation can be vertically averaged without generating spurious dispersive terms, are generally valid.

2.1. The Saint–Venant equations

The Saint–Venant equations describe conservation of mass (continuity, (1)) and momentum (2) in a depth-averaged flow as follows:

$$\frac{\partial h}{\partial t}+\frac{\partial q_x}{\partial x}=cP(t)-I(t) \tag{1}$$

$$\frac{\partial q_x}{\partial t}+\frac{\partial}{\partial x}\left(\frac{q_x^2}{h}+\frac{gh^2}{2}\right)+gh(S_f-S_0)=0 \tag{2}$$

In these equations, t is time, x is the spatial coordinate, h is the ponded water depth, $q_x = Vh$ is the flow rate in the x direction, V is the depth averaged velocity, g is gravitational acceleration, $P(t)$ is rainfall, $I(t)$ is the infiltration rate, S_0 is the ground slope and S_f is the friction slope. All symbols used in the text are summarized in Table 1. We ignore the role of interception in changing rainfall fluxes at vegetated sites ($c = 1$ throughout) given that plant canopies in arid systems are generally sparse, displaying functional adaptations to reduce infiltration losses or to promote the delivery of rainfall to the soil surface [30,31]. Parameterizations of the friction slope in the momentum equation (2) are commonly obtained from the Darcy–Weisbach equation assuming the flow is locally uniform, giving:

$$S_f\approx\frac{f}{8g}\frac{q_x^2}{h^3} \tag{3}$$

where f is the Darcy–Weisbach friction factor. An expression for f that accounts for the effects of vegetation on the flow hydraulics is developed later.

2.2. Approximations to the Saint–Venant equations

Several existing ecohydrological models describing water redistribution in arid or semi-arid environments have been proposed that are driven by simplified versions of the Saint–Venant equations [6,8,25,26]. These simplifications are based on retaining the unsteady contribution in the conservation of mass equation but invoking a steady-state assumption for the momentum equation ($\partial q_x/\partial t = 0$) at small Froude numbers (i.e. $q_x^2/h \ll gh^2/2$) resulting in:

$$\frac{\partial}{\partial x}\left(\frac{gh^2}{2}\right)+gh(S_f-S_0)\approx 0 \tag{4}$$

giving $S_f \approx S_0 - \partial h/\partial x$. If S_f is related to q_x via the Darcy–Weisbach equation (c.f. Eq. 3) then the momentum equation reduces to:

$$S_0-\frac{\partial h}{\partial x}\approx\frac{f}{8g}\frac{q_x^2}{h^3} \tag{5}$$

Table 1
Table of symbols used.

Symbol	Definition
α	Bare soil infiltration rate, cm/h
α_m	Parameter in generalized momentum equation
β	Momentum absorption coefficient
β_m	Parameter in generalized momentum equation
b	Exponent of vegetation–infiltration relation
C_d	Drag coefficient
d	Zero plane displacement (m)
f, $f_{turbulent}$	Darcy–Weisbach friction factor
$f_{viscous}$, f_b, f_v	For turbulent, laminar, vegetated or bare soil cases
F, F_b, F_v	Cumulative infiltration, over bare soil, over vegetation (mm)
$G(h)$	Infiltration dependence on ponded depth
h	Ponded depth (mm)
H_c	Vegetation canopy height (m)
I_c(t)	Infiltration capacity (cm/h)
k	von Karman's constant
λ	Sensitivity of infiltration capacity to vegetation cover
L	Infiltration adjustment length (m)
l_c	Adjustment length scale (m)
LAI	Leaf area index
M	Domain size (m)
$P(t)$	Precipitation intensity (cm/h)
q_x	Flow rate in the x direction (m^3/s)
Re	Reynold's number
S_0	Topographic slope
S_f	Friction slope
t	Time (s)
V	Bulk (depth averaged) fluid velocity (m/s)
x	Cartesian coordinate aligned along the longitudinal dimension (m)
z_o	Momentum roughness length (m)

In almost flat terrain where $S_0 \ll \frac{\partial h}{\partial x}$, q_x can be expressed as

$$q_x = \sqrt{\frac{8g}{f}} h^{\alpha_m} \left(\frac{\partial h}{\partial x}\right)^{\beta_m} \tag{6}$$

and the conventional 'rating curve' or 'flow-depth' relationship derived solely from Manning's equation is recovered if $\alpha_m = 3/2$ and $\beta_m = 1/2$. Two other simplifications can be used: (i) $\alpha_m = 0$ and $\beta_m = 1$, a linear-diffusion case where the dependence on h is all lumped into f. This dependence is admittedly weak when h is much greater than z_o, where z_o is the momentum roughness length characterizing the bed surface. The linear diffusion assumption recapitulates that used in most existing patchy-vegetation models [6,8,25,26]. (ii) $\alpha_m = 3/2$ and $\beta_m = 1$, hereafter referred to as the 'nonlinear-diffusion' case because it assumes $q_x \propto \partial h/\partial x$ via an h-dependent diffusivity. This representation provides a balance between including the full non-linearities of the shallow water equations and the simpler behavior of the linear diffusion case. Note that the assumption that $\partial q_x/\partial t = 0$ is questionable under the conditions of abrupt and intense storms, as might be expected in arid environments, motivating the need to undertake a quantitative comparison between the various flow routing approaches.

2.3. Surface resistance and the Darcy–Weisbach friction factor f

Determining the most important causes of energetic losses in these shallow flow regimes is non-trivial. In examining similar flow regimes, Roche et al. [32] concluded that 'although local Reynolds number values do not clearly indicate that the flow is turbulent … head losses … are dominated by inertia' [32, p. 10]. Rainsplash will tend to agitate the flow, contributing to a disturbed state resembling a turbulent regime [33]. Parameterizing frictional losses associated with laminar flow in shallow overland flow is also problematic, and practical approaches are often based on extrapolation of Poiseuille's equation for laminar flow in pipes, resulting in $f = 64/Re$ where Re is the Reynold's Number, $Re = hV/\nu$, and ν is the kinematic viscosity of water. This extrapolation, however, rarely performs well in capturing the relationship between Reynold's number, roughness and bulk velocity [34,35] primarily due to the highly disturbed state of the boundary layer over these roughness elements. Given the uncertainty regarding the validity of the Poiseuille approximation for these shallow flows, the majority of the analysis here is based upon the assumption that the turbulent stresses are the dominant contributor to f and that laminar stresses can be omitted when the turbulent stresses are considered. That is, we make the reasonable assumption that the turbulent intensity of the shallow flows is high, even when the bulk velocity is low. To explore the implications of this assumption, we also include a treatment in which the turbulent stresses are ignored and only the laminar stresses as given by $f = 64/Re$ are included. For the very shallow depths of flow that arise in this problem, this approximation is likely to induce such large stresses as to render the water virtually stationary and in many cases reduce the problem to a close approximation of one dimensional infiltration. Thus, a focus on the turbulent case allows us to explore a limiting scenario with the maximum water redistribution.

2.3.1. Turbulent flow

The surface resistance f is a nonlinear function of h, and these functions differ for the case of flow over bare soil versus through emergent vegetation. In the case of bare soil, the depth dependence of the Darcy–Weisbach friction factor is the classical 1/7 power law [36–39]. Note that this is a deep layer formulation that assumes that a momentum roughness height $z_o < h$:

$$\sqrt{\frac{f}{8}} \approx 0.18 \left(\frac{z_o}{h}\right)^{1/7}. \tag{7}$$

In the presence of vegetation, two different regimes must be specified for the cases where the flow depth h exceeds the vegetation canopy height H_c, and where the canopy is emergent, i.e. $h/H_c < 1$. For the former case:

$$\sqrt{\frac{f}{8}} = 2\beta \frac{l_c}{H_c}\left(1 - \exp\left(-\frac{1}{2\beta^2}\frac{H_c}{l_c}\right)\right) + \frac{1}{k}\left(\frac{h}{H_c} - 1\right) \times \left[-1 + log\left[\left(\frac{h-d}{z_o}\right)^{\frac{h-d}{h-H_c}} \left(\frac{H_c - d}{z_o}\right)^{-\frac{H_c-d}{h-H_c}}\right]\right] \tag{8}$$

while for $h/H_c < 1$,

$$\sqrt{\frac{f}{8}} = 2\beta \frac{l_c}{h} \exp\left(-\frac{1}{2\beta^2}\frac{H_c}{l_c}\right)\left(-1 + \exp\left(\frac{1}{2\beta^2}\frac{h}{l_c}\right)\right), \tag{9}$$

where $\frac{d}{H_c} = 1 - \frac{2\beta^3 l_c}{kH_c}$, $\frac{z_o}{H_c} = \frac{2\beta^3 l_c}{kH_c} \exp\left[\frac{-k}{\beta}\right]$, $\beta = min\left(0.135\sqrt{\frac{LAI}{H_c}}, 0.33\right)$ and $l_c = \left[C_d \frac{LAI}{H_c}\right]^{-1}$. The full derivation of these equations is presented elsewhere [40].

The zero-plane displacement d and momentum roughness height z_o for the vegetation both vary with the geometric properties of the canopy, while β, the momentum absorption coefficient varies with the leaf area density. The adjustment length l_c measures how rapidly the wakes generated by the vegetation dissipate turbulent kinetic energy from the flow. The k is Von Karman's constant, and the C_d is the dimensionless foliage drag coefficient. In all these formulations, we assumed that the leaf area density was uniform with height, and was well approximated by the leaf area index (LAI) divided by the canopy height (H_c). When the drag force exerted by the vegetation on the flow is dominated by form – rather than viscous-drag, C_d is constant. In practice, the different nonlinear dependence of f on h for bare soil (f_b) and vegetated (f_v) conditions results in two outcomes: (a) $f_v > f_b$, and (b) the

dependence of f_b on h saturates at much lower values of h than does f_v.

2.4. Infiltration behavior

A recent meta-analysis of biomass-infiltration capacity relationships across nearly 50 vegetation communities [14] indicated that in arid ecosystems, vegetation provides a first order control on infiltration capacity, with the dependence of infiltration capacity on vegetation describing a power-law relationship with above-ground biomass. Here, the leaf area index (LAI) is used as a surrogate for above ground biomass, allowing the infiltration capacity to be expressed as:

$$I_c(t) = \alpha(1 + \lambda LAI^b)G(h) \tag{10}$$

where α indicates the infiltration capacity of bare soil, λ a proportional enhancement associated with vegetation, and $b \approx 0.4$ based on empirical data [14]. The multiplier $G(h)$ is used to alternate between the depth-dependent infiltration case used in vegetation patterning models, $G(h) = h/z_o$, and a classical description of infiltration where $G(h) = 1$. To allow the two cases to be directly compared we choose the baseline infiltration rate α so that I_c is equal for the depth-dependent and depth-independent cases when the depth of ponding is equal to the bare-soil momentum roughness height, $h = z_o$. This matching is necessary to ensure that the maximum ponded depths generated in the two cases are comparable. The sorptive effects of the crusted soils were assumed to be small so that infiltration capacity could be assumed to be entirely gravitational.

3. Numerical experiments

To address the research questions posed in the introduction, Eqs. (1)–(6) were solved numerically on a flat, 1D domain, 300 m in length (the scale illustrated in Fig. 1). The left hand side of the domain (0–150 m) was treated as a bare soil condition covered by crusted soils, while the right hand side of the domain (150–300 m) was assumed to be covered by uniform vegetation. The frictional resistance to flow (roughness) in bare areas was computed with Eq. (7), assuming $z_o = 0.001$ m, i.e. a 1 mm grain roughness, comparable to a flat sandy surface. The roughness in vegetated areas was computed with Eq. (9). No-flux boundary conditions were applied at the lateral boundaries assuming the domain could be viewed as part of a repeating periodic vegetation pattern. We tested the sensitivity of the results to these spatial parameters by varying the proportion of the surface that was vegetated between 25% and 75%, and by shrinking the domain size by an order of magnitude to 30 m. These changes in percentage vegetation cover span the observed variation in the scales of periodic vegetation patterns observed in the field. Rainfall and infiltration properties were chosen to reflect realistic but limiting cases: 1.0 cm/h infiltration capacity for bare soils (c.f. [15]) and storm intensities ranging from 1.1 to 7 cm/h. These intensities span a range from the lowest-intensity storms that could generate ponding given the soil infiltration capacities (comparable to storms with < 1 year return intervals); to intensities comparable to a 5-year storm, assuming storm durations of 30 min (intensity-frequency-duration data taken from cyclonically/monsoonally influenced desert ecosystems, [41]). For the infiltration cases where $G(h) = h/z_o$, infiltration rates asymptote to zero as the soil surface dries. In these cases the numerical runs were terminated when the ponded volume on the soil surface was <1% of the total precipitation volume. Otherwise, simulations ended when the total ponded volume became zero. Parameters for the numerical experiments are summarized in Table 2.

4. Results

The results are organized around the two research questions posed in the introduction. Results are presented in terms of cumulative infiltration (F, where F_v and F_b are used to represent the cumulative infiltration per unit area for vegetated and bare soil sites, respectively). These values are referenced to each other and to the total (cumulative) rainfall depth per unit area, P_{tot} (mm). Unless otherwise stated, the results assume that turbulent stresses are dominant.

4.1. Can contrasts in infiltration rate and surface roughness lead to a lateral redistribution of water from bare to vegetated sites?

All the model runs were compared to a reference case in which there was no contrast in the infiltration capacity between the bare and vegetated sites (i.e. $\lambda = 0$), and both were treated as the bare case. In this situation, the cumulative infiltration $F_v = F_b = F$ independent of any other parameter choice and the 1D infiltration situation is recovered. However, when a contrast in roughness and infiltration was present, then differences in the ponded depth between the bare and vegetated sites develop, as illustrated in Fig. 2. These differences generate lateral flow from bare sites to vegetated sites. The effect of this flow is to enhance the water available at the vegetated site beyond that provided by rainfall, and to reduce water availability at the bare site to less than that provided by rainfall. As illustrated in Fig. 3, this enhancement is dependent upon the storm intensity, the sensitivity of the infiltration behavior to the presence of vegetation (λ) and the assumptions made about the infiltration dependence on ponded depth. For h-dependent infiltration (i.e. $G(h) = h/z_o$), the behavior of this 'lateral water subsidy' provided to the vegetated sites in addition to rainfall is consistent, regardless of rainfall intensity, at ≈20% ($\lambda = 2$) or ≈30% ($\lambda = 4$). For h-independent infiltration (i.e. $G(h) = 1$), the subsidy is strongly and nonlinearly-dependent on the rainfall intensity, and ranges from 0 to 40% of the rainfall depth. The subsidy was most strongly influenced by the infiltration contrast. Although the roughness contrasts generated during the course of the simulations ranged over an order of magnitude, with $f_b \approx 0.3$ and $f_v \approx 5$ as shown in Fig. 2, removing this contrast and setting $f_v = f_b$ only increases the cumulative infiltration by a factor of 10% for the heaviest storms and h-independent infiltration (see Supplementary Fig. 1), which is comparable to increasing the infiltration contrast by a factor of 2 (see Fig. 3). Furthermore, this sensitivity to the roughness decreased as the infiltration contrast increased, suggesting that it is most important for low surface gradients.

The water contributed to the patch by lateral flow does not infiltrate uniformly across the vegetated site but is concentrated at the bare-soil – vegetation boundary. As shown in Fig. 4, the profile of the lateral distribution of infiltrated water is invariant in the case of h-dependent infiltration, but varies with intensity where infiltration is independent from h. In this case, the center of the patch is only subsidized by lateral redistribution for the most intense and infrequent storms. By computing the spatial gradient of the cumulative infiltration volume, a region can be defined where $|\partial F/\partial x| > \epsilon$, where $\epsilon = 0.001 \max|\partial F/\partial x|$. As illustrated in Fig. 5, panel D, this is the region where the presence of the soil-vegetation contrast appreciably alters the local infiltration due to the action of lateral flow. This region can be quantified by a length-scale L (defined as the length of the region where $|\partial F/\partial x| > \epsilon$), termed the infiltration adjustment length. L defines the component of the bare soil region that contributes water to the vegetated patch via lateral flow, and the component of the vegetated patch which receives this redistributed water as infiltration. In the same way that the redistrib-

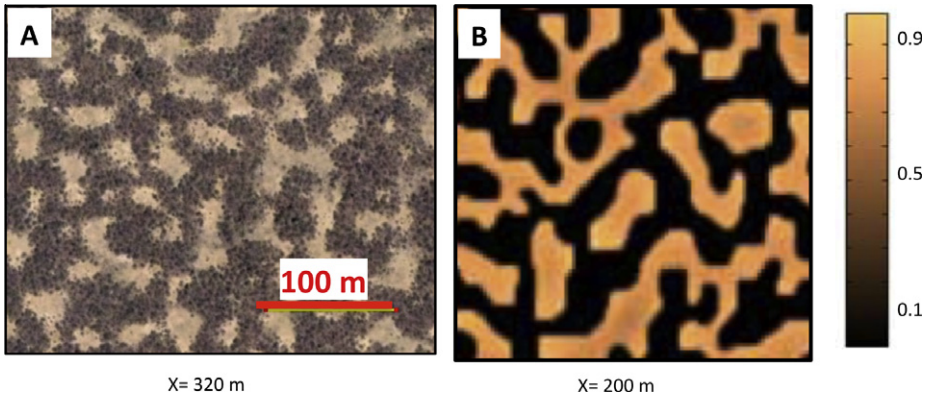

Fig. 1. (A) Runon–runoff dynamics are hypothesized to contribute to the persistence of patchy arid ecosystems such as these found in South-Eastern Niger, 12°19′54.91″N, 3°10′41.76″E. Image from Google Earth. Copyright 2011 Digital Globe. (B) By assuming that infiltration scales linearly with ponded depth, varies with local vegetation cover, and that flow can be approximated by a diffusion equation, simple models reproduce the morphology of observed vegetation patterns. The color scale is proportional to local biomass density, normalized between 0 (bare soil) and 1 (complete vegetation cover). *Source*: Example taken from [45].

Table 2
Parameters for the model simulations. Where more than one parameter or model component is listed, the cases were run factorially to explore all combinations of parameters.

Model component	Value(s)
Infiltration model	$G(h) = h/z_o$ or $G(h) = 1$
Hydraulic model	Saint–Venant equations, Mannings equation, Nonlinear diffusion, Linear diffusion
Infiltration contrast λ	0 (no contrast), 2, 4
Base infiltration rate (α, cm/h)	1.0 cm/h
Roughness contrast (bare soil to vegetated)	Laminar f (no contrast, or 64/Re) or Turbulent f (no contrast, or Eq. (9))
Rainfall intensity (cm/h)	1.1, 1.5, 2.5, 5, 7 cm/h
Rainfall duration (min)	30
Roughness length (z_o, mm)	2
Drag coefficient (C_d, –)	0.2
Canopy height (H_c, m)	0.1 (always greater than ponded depth)
Leaf density [m^2/m^3]	10

uted water is distributed non-uniformly across the vegetated patch, it is apparent that the loss of water to the lateral subsidy occurs non-uniformly across the bare patch, with the subsidy being strongest immediately adjacent to the patch boundary (see Fig. 5).

In practice L for the h-dependent infiltration always extends to the domain boundary (Fig. 5 Panel C), implying that all of the bare soil area contributes to the lateral flux, and all of the vegetated patch receives a lateral subsidy. However, the infiltration adjustment length for h-independent infiltration is a function of the rainfall intensity (Fig. 5 Panels A and B). Where $L \ll M$ with M representing the size of the domain, alterations to the spatial configuration of vegetation and soil, or to the size of the vegetated patch, adjust the importance of the subsidy in trivial ways only. That is, although the ratio of F_v to P_{tot} increases as the size of the vegetated patch shrinks, this simply reflects that a relatively larger proportion of the vegetated patch is spanned by L (c.f. Fig. 5 panel A). A fixed bare soil area contributes to the lateral fluxes, and a fixed vegetated area receives the subsidy, and the F_v to P_{tot} ratio only reflects the magnitude of the subsidized area to the whole vegetation patch. However, as P rises, L increases to the point where it spans the domain and interacts with the domain boundary (c.f. Fig. 5 panel B). This interaction not only increases the proportion of the vegetated patch spanned by L, but also the magnitude of the subsidy to the patch, due to water backing up from the no-flow condition at the boundary. Thus the boundary condition interaction leads to a greater subsidy effect for a 75% bare area when $P = 7$ cm/h (Fig. 5 panel B) but not when $P = 1.1$ cm/h (Fig. 5 panel A). The flow-boundary interaction is reflected in the nonlinear dependence of the subsidy on the patch size for increasing rainfall intensities (Table 3). In the case of h-dependent infiltration, the boundary conditions influence ponded water redistribution for even the lowest intensity storms. However, these effects are invariant with storm size, meaning that the proportional changes in lateral redistribution induced by the patch area are insensitive to the rainfall intensity (Table 3). As the rainfall intensity increases, the infiltration adjustment length increases in a near linear fashion until $L \approx M$ at which point the boundary conditions interact sensitively with the infiltration behavior (see Fig. 5 panel D).

This analysis suggests that the infiltration adjustment length L is a key length-scale dictating the infiltration behavior in the systems where infiltration behaves in an h-independent fashion. The sensitivity of L to P appears to be near-linear. As the infiltration contrast increases, L grows more slowly with P: $L \propto 105P$ for $\lambda = 2$ but $L \propto 51P$ for $\lambda = 4$. The infiltration adjustment length is insensitive to the presence of a roughness contrast in f_b and f_v. It is however sensitive to the assumptions about the parameterization of the stresses, and L is constrained at low Reynolds numbers under the assumption that $f = 64/Re$.

The emergence of L as a key length scale determining the redistribution of water suggests that adjustments to the spatial scale of the domain M could ensure that all the bare soil area contributes to the lateral flow, and that all the vegetated patch benefits from the redistribution. Assuming L is approximately symmetric across the plant-soil boundary, this optimization would be achieved when $M < L$, with the L value derived from the average properties of the storms that generate lateral flow at any given location. Based on observations of patchy vegetation, a reasonable 'lower bound' on the patch size is approximately 30 m, compared to the 300 m previously assumed. Re-running the model results suggests that the degree of subsidy for $M = 300$ or $M = 30$ is virtually unchanged for low intensity storms. As the storm intensity increases lateral transport for $M = 30$ is enhanced relative to $M = 300$, and rainfall subsidies increase by approximately 15% (h-independent infiltration). The enhancement of infiltration subsidies was damped for the case of h-dependent infiltration (presumably because the boundary condition influenced water redistribution in both the 30 and 300 m domains) with a ≈3% enhancement of infiltration.

The results discussed above assume that the two-dimensional form of the patches can be locally approximated as a linear vege-

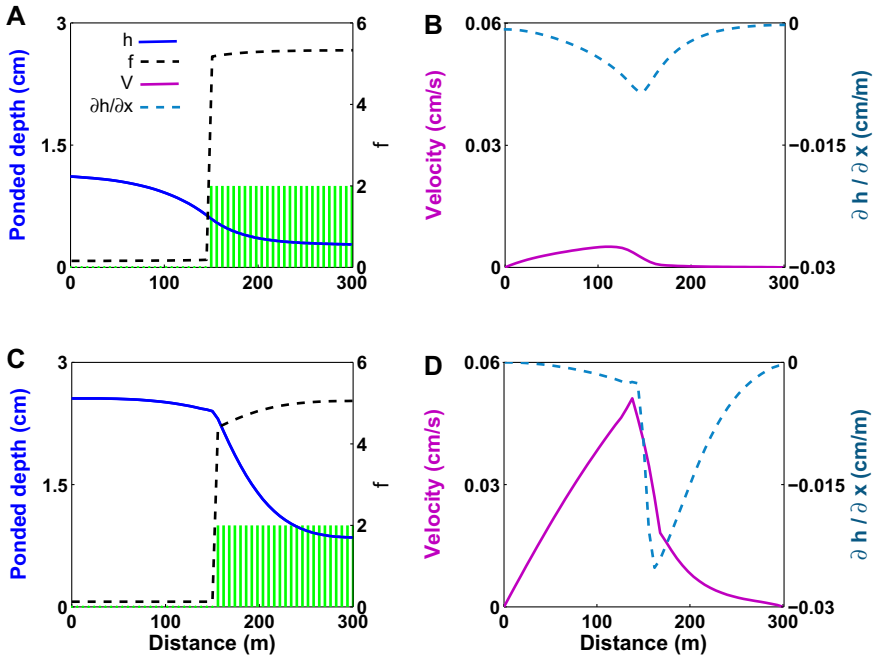

Fig. 2. Examples of the computed profiles of ponded water depth, friction factors, the surface water slope and the flow velocities at the end of a 30 min 7 cm/h storm event for (A) and (B) *h*-dependent infiltration and (C) and (D) *h*-independent infiltration. Panels (A) and (C) show the ponded depth (blue, left axis) and the friction factors (black dashed lines, right axis). The green bars indicate the vegetated region. Panels (B) and (D) show the flow velocity (with the positive direction being from left to right) (pink, left axis) and the surface water gradients (light blue dashed lines, right axis). Note that the peak flow velocities do not coincide with the maximum surface gradients because of the higher resistance generated by vegetation. (For interpretation of the references to colour in this figure legend, the reader is referred to the web version of this article.)

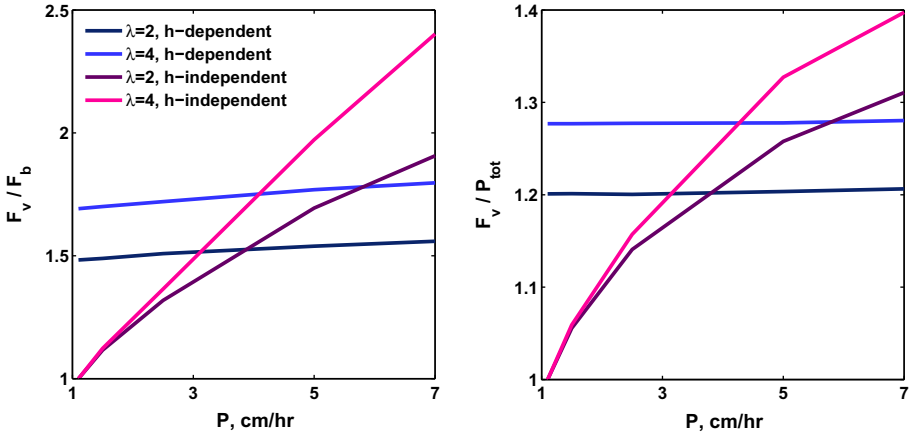

Fig. 3. Contrast in cumulative infiltration between bare soil and vegetated sites as a function of the infiltration contrast λ, the infiltration behavior (*h*-dependence or independence) and the rainfall intensity. (B) Relative enhancement of vegetation water availability over rainfall as a function of infiltration contrast and infiltration behavior.

tated band, a reasonable assumption for 'labyrinthine' or 'gapped morphologies' [8]. For isolated, near-circular patches of vegetation, however, the ratio of the patch area to the length of the patch edge is much smaller. When $M = 300$, such circular morphology would increase the water availability by ≈35% or ≈48% over rainfall for an *h*-dependent infiltration case (for $\lambda = 2$ and $\lambda = 4$), or by as much as 62% of rainfall depth for *h*-independent infiltration with $P = 7$ cm/h and $\lambda = 4$. The most efficient water transfer scenario we considered consists of circular patches, occupying 25% of the domain, with a 'short' wavelength of 30 m. Under these conditions, the total lateral subsidy amounts to an additional 110% of the rainfall received by the patch. This is consistent with the observations of patchy vegetation forming isolated 'spot' patterns in very dry climates [8].

4.2. How sensitive are the predictions about the lateral redistribution to the assumptions made about infiltration, roughness, and to the choice of hydraulic model used to parameterize the flow?

As illustrated in Fig. 3, the assumptions about infiltration behavior were the dominant factor in determining the redistribution of water for cases where it is assumed that the stresses are fully turbulent. Changes in infiltration behavior altered the sensitivity of the redistribution to the rainfall intensity, and altered the magnitude of the redistribution by factors of up to 100%. By comparison, doubling the infiltration sensitivity to the presence of vegetation (i.e. altering the infiltration contrast by ≈70% for the parameters chosen) resulted in only a 10% change in the volume of water infiltrated over the vegetated patch. If the roughness

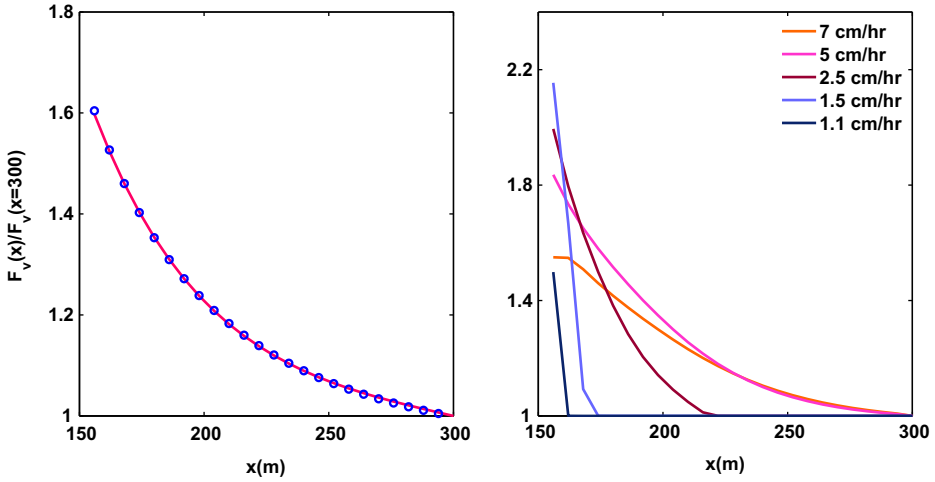

Fig. 4. Normalized cumulative infiltration ($F(x)^* = F(x)/F(x = 300)$) over the vegetated sites. (A) For h-dependent infiltration, all curves collapse to a single power law relationship of the form $F(x)^* = 5.4 \times 10^6 x^{-3.142} + 0.91$. Some lateral transfer occurs at all scales. (B) For h-independent infiltration the lateral extent of the subsidy depends on the intensity of rainfall and is constrained to less than the full width of the vegetated patch for intensities of 2.5 cm/h or less. As rainfall intensities increase, a greater proportion of the lateral subsidy extends to the boundary (at $x = 300$ m), and consequently the infiltration contrast through space- or the magnitude of the $F(x)^* = F(x)/F(x = 300)$ line plotted here – declines as the intensity increases.

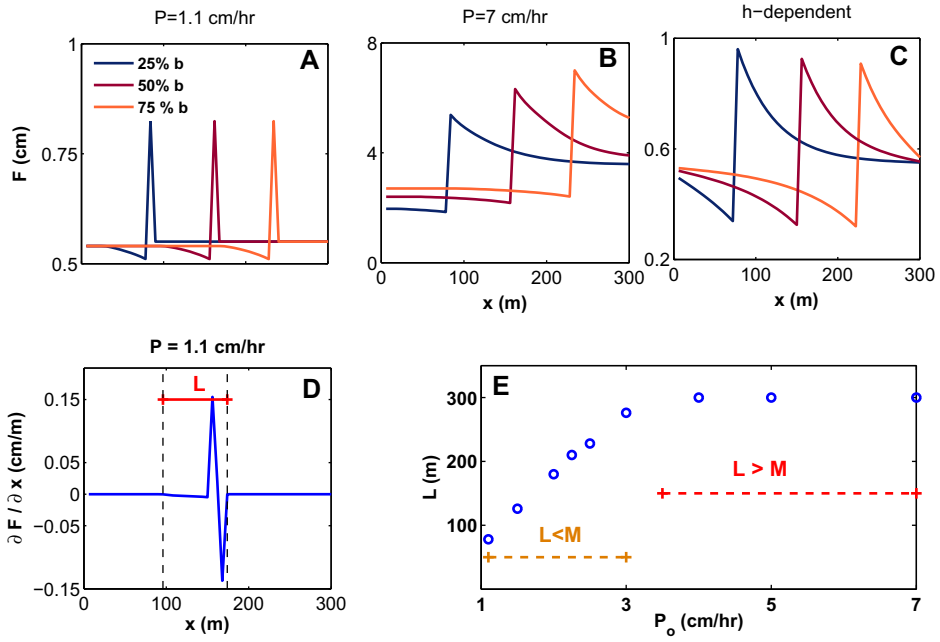

Fig. 5. Sensitivity of the infiltration behavior to the spatial organization of the domain. (A)–(B) show the behavior of h-independent infiltration for rainfall rates of 1.1 cm/h (A), and 7 cm/h (B). The distribution of infiltration through space responds sensitively to the changes in rainfall intensity. 'b' indicates the percentage of the domain set to bare soil conditions. (C) shows a single case of h-dependent infiltration ($P = 1.1$ cm/h) which exhibited spatially similar behavior regardless of the rainfall intensity. (D) shows the definition of the adjustment length L, as the region over which $|\partial F/\partial x| > \epsilon$. (E) indicates the behavior of L as the rainfall intensity P is increased. Two regions emerge: one in which L increases in a near-linear fashion and is less than the domain width M. Once L grows to greater than M the perturbed region spans the domain and no longer changes with rainfall intensity.

contrast was eliminated altogether, the increase in the lateral redistribution of water to the vegetated patches was negligible for h-dependent infiltration and only increased by 10% for h-independent infiltration (see Supplementary Figs. 1 and 2). These sensitivities were not strongly contingent on the patch sizes.

If laminar stresses were included under the assumption that these could be represented as $64/Re$, there was no discernible effect on the spatial distribution of cumulative infiltration in the h-dependent case (that is, for $\lambda = 2$, $F_v/P_{tot} = 1.2$ for all rainfall intensities. There were large effects on the h-independent case however, with the presence of laminar stresses greatly reducing the subsidy of water to the vegetated sites. The maximum values of $F_v/F_b = 1.2$ in the laminar case compared to 1.9 in the turbulent case, and the maximum value of $F_v/P_{tot} = 1.1$ for the laminar case compared to 1.3 in the turbulent case (to compare values for all rainfall intensities, see Supplementary Fig. 3).

The choice of hydraulic model used to describe the flow behavior also introduced differences in the predictions of water subsidy to the vegetated patch, as shown in Fig. 6. Deviations on the order of 5–20% from the predictions of the Saint–Venant equations were

Table 3
F_v/P_{tot} reported for five different rainfall intensities and three different patch sizes. '*b*' indicates the bare soil area, and '*v*' the vegetated area.

P (cm/h)	25:75 *b*:*v* M = 300 m	50:50 *b*:*v* M = 300 m	75:25 *b*:*v* M = 300 m	50:50 *b*:*v* M = 30 m
h-Independent infiltration				
1.1	1.01	1.02	1.12	1.02
1.5	1.05	1.06	1.24	1.09
2.5	1.10	1.12	1.42	1.26
5	1.14	1.23	1.67	1.39
7	1.15	1.28	1.82	1.41
h-Dependent infiltration				
1.1	1.21	1.21	1.48	1.24
1.5	1.21	1.21	1.49	1.25
2.5	1.21	1.21	1.49	1.25
5	1.21	1.21	1.49	1.25
7	1.21	1.21	1.49	1.25

associated with the use of linearized or simplified flow models. These errors are comparable to the magnitude of the enhancement of infiltration in the vegetated sites induced by the soil contrast (c.f. Fig. 3). The exception is the linear diffusion model in combination with *h*-dependent infiltration, which reproduces the predictions from the Saint–Venant equations closely. Coincidentally (and fortunately), this is the combination of infiltration and hydraulic assumptions used in the majority of patchy arid ecosystem models [6,8,25,26], suggesting that the choice of a simplified hydraulic model is unlikely to have significantly biased the predictions of these models in situations where h-dependent infiltration occurs.

5. Discussion and conclusion

The analysis here suggests several broad conclusions: firstly that on flat sites, the infiltration contrast can induce significant lateral transport of water during storm events, secondly that the nature of the infiltration assumptions and infiltration contrast are the most significant controls on this transport, with the hydraulic factors such as surface roughness acting as secondary effects, and finally that the redistribution behavior can be approximated by a lengthscale that appears to increase in a near-linear fashion with the rainfall intensity.

Applying a simple scale analysis to the steady-state Saint–Venant momentum equation allows us to briefly explore these limitations of validity for this analysis. For instance, from the results of the simulations shown in Fig. 2, the peak magnitude of $\frac{\partial h}{\partial x}$ can be estimated as approximately 5 mm over 50 m, or a 0.1% slope. Where bed slopes were much greater than 0.1%, the bed slope terms would dominate over the free surface gradient and a more conventional hydraulic analysis should be applied. Therefore, 'flat' in this context is bounded by slopes on the order of 0.1%, or around 0.1°.

The model results have several implications for understanding the dynamics of water redistribution in patchy arid ecosystems. Firstly, they suggest that even during intense storms on soils with a strong infiltration contrast, the total volume of water redistributed laterally due to the slope produced by the free water surface is a relatively small fraction of rainfall. No simulation suggested more than a 110% enhancement of water availability (i.e. $F_v/P_{tot} = 2.1$) in the vegetated sites, and then only for the largest and least frequent storms and with bare soil covering 75% of the domain. This is much smaller than the reported enhancements in water stored in the soil profile beneath vegetated sites on slopes (up to eight times the volume of annual rainfall as reported by Galle et al. [42] for sloping sites in the Sahel, where redistribution contributed approximately four times more water to the vegetated zone annually than did rainfall). The relatively small increases in water availability introduced in this setting suggest that, with the possible exception of sites where vegetation grows in very small, circular patches, it would be sensible to consider that surface redistribution of water operates in conjunction with other facilitative processes to sustain vegetation. This is particularly likely to be true in situations where microtopographic variation exists between bare and vegetated sites, since microtopographic variability is likely to impede lateral redistribution, or at least to confine redistribution strongly to the edges of vegetated mounds. This conclusion broadly supports the likely importance of belowground processes (i.e. redistribution of infiltrated water across the plant root system) and the plant structural parameters for sustaining vegetation growth in flat sites as suggested by Lefever et al. [7]. This would also be consistent with the observations of vegetation patterning arising in locations where no infiltration contrast is present [5], and raises the possibility that different facilitative processes may sustain vegetation patches in sloping versus topographically flat sites.

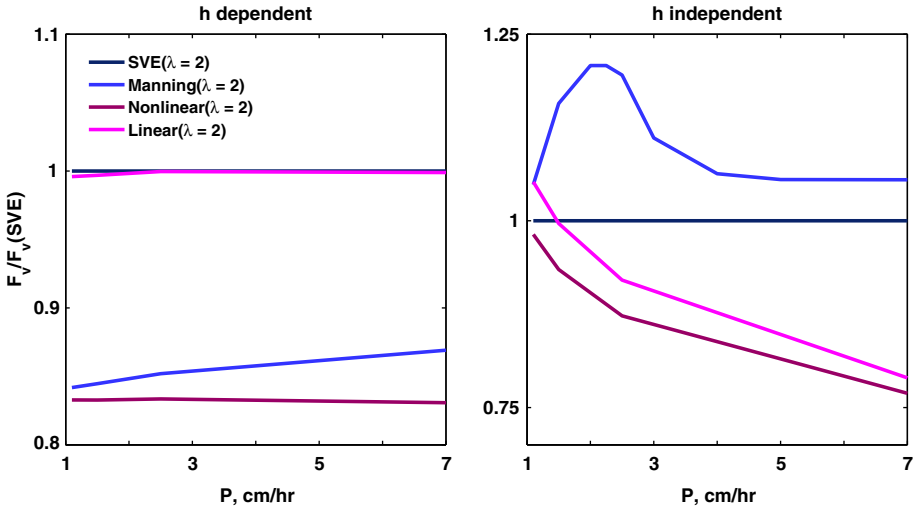

Fig. 6. Cumulative infiltration in the vegetated zone as computed using three simplifications to the Saint–Venant equations, relative to the cumulative infiltration computed by the complete Saint–Venant equations. Note that where infiltration was proportional to ponded depth, the linear diffusion approximation provided an excellent estimate of cumulative infiltration in the vegetated sites, while a rating curve or a nonlinear diffusion approximation induced 15–20% error. Where infiltration was independent of depth, the error in each of the models ranges between 5% and 20%.

The 20–60% increases in water availability attributable to run-on–runoff mechanisms in sites with approximately 50% plant cover (c.f. Fig. 2), while likely insufficient to fully explain the patchiness of dryland vegetation, would contribute to the survival and growth of vegetation within patches, particularly at the edges. They may, for instance, explain the presence of a zone of annual plant growth often reported at the edge of vegetated patches [4]. It is also in this zone that the roughness of the vegetated sites has its most pronounced effects, particularly for larger storm events, with increasing roughness tending to isolate the contribution of redistributed water close to the edge of the patch (see Supplementary Fig. 2). The importance of the lateral contribution will depend on the statistics of rainfall and the infiltration properties at a site. For instance, taking 20 years of rainfall statistics from Menindee, Australia, where vegetated patches form on plains with slopes as low as 0.1%, [43,15] and simply weighting the events by frequency, we would predict that on average lateral subsidies contribute some additional 26% of rainfall – or approximately 70 mm/year to the maintenance of these vegetated sites (storms with intensities of over 1.0 cm/h contributed 98% of all rainfall at this site).

Secondly, the results suggest that to draw firm conclusions about the dynamics of water redistribution in topographically flat sites with contrasting soil properties, two aspects of the hydraulics must be better constrained. The first of these relates to the potential links between the depth of ponded water and the dynamics of infiltration. Classical infiltration theory suggests that the spatial partitioning of rainfall would be strongly dependent on storm intensity and the nature of the dominant stresses in the fluid (turbulent vs. laminar). If, however, infiltration rates are phenomenologically dependent on water depth, reflecting small scale microtopographic variations or surface cracking [29,27], the dynamics become relatively independent of rainfall intensity and other hydraulic assumptions. This is because an h-dependence of the infiltration behavior means that a pseudo-steady ponded water condition exists at which the infiltration rate approximately balances the rainfall intensity. The implications of such a pseudo-steady state are that (a) water ponds across the entire profile, (b) the total variability in the ponded depth across the range of rainfall intensities tested is constrained: a factor of six variation in comparison to a ≈60-fold variation for the h-independent case; and (c) the proportional contrast in ponded depth between the vegetated and unvegetated sites is independent of the rainfall intensity (at steady state). This convergence to a constant contrast in ponded depth is the dominant feature of the dynamics of the h-dependent simulations, causing the rainfall spatial partitioning to be relatively independent of assumptions about roughness, laminar or turbulent flow regime, or the imposed rainfall variability. The potential for the h-dependent infiltration dynamics to reach a steady state may also explain why the linear diffusion model, which is based on the assumption of steady-state inertial terms, was able to reasonably reproduce the results of the Saint–Venant equations. By comparison, the h-independent infiltration is always transient, and often leads to low ponded depths. These low ponded depths significantly slow the lateral water flux due to the feedback between depth and flow rate. Consequently the redistribution behavior is much more sensitive to assumptions about roughness and flow regime in such a setup, and deviations between the Saint–Venant results and those of the simplified flow models were always observed.

The sensitivity to the specification of the roughness and flow motivates the need to further investigate the nature of the stresses opposing lateral flow. As identified above, the assumption that all stresses are laminar results in a very effective inhibition of lateral fluxes for all but the largest storms, and significantly inhibits the capacity of infiltration contrasts to promote spatial partitioning of infiltration volumes on flat terrain. Ascertaining the appropriate parameterization of laminar stresses with respect to the Reynolds Number is a necessary step to refining estimates of the significance of overland flow. Considerable uncertainty still prevails in the literature as to the appropriate way to model the stresses in partially inundated shallow flow over a rough boundary [34,32,24]. Experimental investigations for this specific orientation of bare soil and vegetation are likely to be the most appropriate way forward.

The modeling study suggests that for the purposes of developing water routing models for patchy arid ecosystems, *if* infiltration exhibits depth dependence, it may be reasonable to replace the solution of the full Saint–Venant equations by a linearized diffusion model [8,26,6,25] without loss of validity of the solution. However, should conventional h-independent infiltration predominate, then neither a rating curve nor diffusive approximations to the Saint–Venant equations can approximate the water redistribution sufficiently well to resolve the behavior predicted by the full Saint–Venant solutions.

The results suggest that one control on the redistribution of water is the infiltration adjustment length L, a hydraulic length scale set by soil and rainfall properties. Where the characteristic length scale of the vegetation – soil spatial patchiness M greatly exceeds L, lateral redistribution of water from bare sites to vegetated sites is sub-optimal, since there are parts of the domain that are not hydraulically influenced by the infiltration capacity contrast. This implies that not all bare soil regions effectively contribute water to the vegetated patch, and portions of the vegetated site do not receive water via run-on. Thus L sets a reasonable upper limit on the spacing of vegetation patches in the landscape. In general we would anticipate that observed patch spacing would be smaller than L. Again using Menindee as an example, we would predict from the rainfall regime that L would be ≈150 m, while typical repeating units in this area are instead found on scales of ≈50–100 m [44].

In closing, the numerical experiments performed here suggest that there are several mechanistic uncertainties regarding the topographically-flat lateral redistribution problem: the behavior of infiltration and the description of the dominant stresses in the fluid. These uncertainties are amenable to experimental investigation, either in field or controlled laboratory conditions (given their physical nature). Clarifying these uncertainties will contribute to understanding the eco-hydrological processes maintaining vegetation growth in patchy arid ecosystems and will facilitate improved eco-hydrological modeling of these systems.

Acknowledgements

The authors acknowledge support from the NSF through EAR – 1013339, the NSF Graduate Fellowship program and the Fulbright Italy distinguished scholars program.

Appendix A. Supplementary data

Supplementary data associated with this article can be found, in the online version, at doi:10.1016/j.advwatres.2011.05.012.

References

[1] Borgogno F, D'Odorico P, Laio F, Ridolfi L. Mathematical models of vegetation pattern formation in ecohydrology. Rev Geophys 2009:47.
[2] Bromley J, Brouwer J, Barker AP, Gaze SR, Valentin C. The role of surface water redistribution in an area of patterned vegetation in a semi-arid environment, south-west Niger. J Hydrol 1997;198(1–4):1–29.
[3] Kefi S, Rietkerk M, Alados CL, Pueyo Y, Papanastasis VP, ElAich A, et al. Spatial vegetation patterns and imminent desertification in Mediterranean arid ecosystems. Nature 2007;449(7159):U213–5.

[4] Seghieri J, Galle S, Rajot JL, Ehrmann M. Relationships between soil moisture and growth of herbaceous plants in a natural vegetation mosaic in niger. J Arid Environ 1997;36(1):87–102.
[5] Barbier N, Couteron P, Lefever R, Deblauwe V, Lejeune O. Spatial decoupling of facilitation and competition at the origin of gapped vegetation patterns. Ecology 2008;89(6):1521–31.
[6] HilleRisLambers R, Rietkerk M, van den Bosch F, Prins HHT, de Kroon H. Vegetation pattern formation in semi-arid grazing systems. Ecology 2001;82(1):50–61.
[7] Lefever R, Barbier N, Couteron P, Lejeune O. Deeply gapped vegetation patterns: on crown/root allometry, criticality and desertification. J Theor Biol 2009;261(2):194–209.
[8] Rietkerk M, Boerlijst MC, van Langevelde F, HilleRisLambers R, van de Koppel J, Kumar L, et al. Self-organization of vegetation in arid ecosystems. Am Nat 2002;160(4):524–30.
[9] Fiedler FR, Ramirez JA. A numerical method for simulating discontinuous shallow flow over an infiltrating surface. Int J Numer Methods Fluids 2000;32(2):219–40.
[10] Giraldez JV, Woolhiser DA. Analytical integration of the kinematic equation for runoff on a plane under constant rainfall rate and Smith and Parlange infiltration. Water Resour Res 1996;32(11):3385–9.
[11] Philip JR. An infiltration equation with physical significance. Soil Sci 1954;77(2):153–7.
[12] Biscarini C, Di Francesco S, Manciola P. CFD modelling approach for dam break flow studies. Hydrol Earth Syst Sci 2010;14(4):705–18.
[13] Khanna M, Malano HM. Modelling of basin irrigation systems: a review. Agric Water Manage 2006;83(1–2):87–99.
[14] Thompson SE, Harman CJ, Heine P, Katul GG. Vegetation-infiltration relationships across climatic and soil type gradients. J Geophys Res Biogeosci 2010;115(G02023). doi:10.1029/2009JG001134.
[15] Dunkerley D. Systematic variation of soil infiltration rates within and between the components of the vegetation mosaic in an Australian desert landscape. Hydrol Process 2002;16(1):119–31.
[16] Vanes HM. Evaluation of temporal, spatial and tillage-induced variability for parameterization of soil infiltration. Geoderma 1993;60(1–4):187–99.
[17] Hallett PD, Nunan N, Douglas JT, Young IM. Millimeter-scale spatial variability in soil water sorptivity: scale, surface elevation, and subcritical repellency effects. Soil Sci Soc Am J 2004;68(2):352–8.
[18] Greene RSB. Soil physical properties of 3 geomorphic zones in a semiarid mulga woodland. Aust J Soil Res 1992;30(1):55–69.
[19] Walsh RPD, Voigt PJ. Vegetation litter: an underestimated variable in hydrology and geomorphology. J Biogeogr 1977;4(3):253–74.
[20] Assouline S, Mualem Y. Modeling the dynamics of soil seal formation: analysis of the effect of soil and rainfall properties. Water Resour Res 2000;36(8):2341–9.
[21] Belnap J. The potential roles of biological soil crusts in dryland hydrologic cycles. Hydrol Process 2006;20(15):3159–78.
[22] Philip JR. Infiltration into crusted soils. Water Resour Res 1998;34(8):1919–27.
[23] Thompson SE, Katul GG, Porporato A. Role of microtopography in rainfall–runoff partitioning: an analysis using idealized geometry. Water Resour Res 2010;46(W07520). doi:10.1029/2009WR008835.
[24] Poggi D, Krug C, Katul GG. Hydraulic resistance of submerged rigid vegetation derived from first-order closure models. Water Resour Res 2009:45.
[25] Meron E, Gilad E, von Hardenberg J, Shachak M, Zarmi Y. Vegetation patterns along a rainfall gradient. Chaos Soliton Fract 2004;19(2):367–76.
[26] Yizhaq H, Gilad E, Meron E. Banded vegetation: biological productivity and resilience. Phys A – Statist Mech Appl 2005;356(1):139–44.
[27] Dunne T, Zhang WH, Aubry BF. Effects of rainfall, vegetation and microtopography on infiltration and runoff. Water Resour Res 1991;27(9):2271–85.
[28] Fox D, Le Bissonais Y, Bruand A. The effect of ponding depth on infiltration in a crusted surface depression. Catena 1998;32(2):87–100. doi:10.1016/S0341-8162(98)00042-3.
[29] Novak V, Simunek J, van Genuchten MT. Infiltration of water into soil with cracks. Journal of Irrigation and Drainage Engineering – ASCE 2000;126(1):41–7.
[30] Martinez Meza E, Whitford W. Stemflow, throughfall and channelization of stemflow by roots in three Chihuahuan desert shrubs. J Arid Environ 1996:271–87.
[31] Domingo F, Sanchez G, Moro MJ, Brenner AJ, Puigdefabregas. Measurement and modelling of rainfall interception by three semi-arid canopies. Agric Forest Meteorol 1998;91(3-4):275–92.
[32] Roche N, Daian JF, Lawrence DSL. Hydraulic modeling of runoff over a rough surface under partial inundation. Water Resour Res 2007;43(W08410). doi:10.1029/2006WR005484.
[33] Brutsaert W. Hydrology: an introduction, vol. 1. Cambridge: Cambridge University Press; 2005.
[34] Lawrence DSL. Hydraulic resistance in overland flow during partial and marginal surface inundation: experimental observations and modeling. Water Resour Res 2000;36(8):2381–93.
[35] Abrahams AD, Parsons AJ, Luk SH. Resistance to overland flow on desert hillslopes. J Hydrol 1986;88(3–4):343–63.
[36] Blasius H. The law of similarity of frictional processes in fluids. Berlin: Wesen; 1913.
[37] Brutsaert W, Yeh GT. A power wind law for turbulent transfer computations. Water Resour Res 1970;6(5):1387–91.
[38] Chen CI. Unified theory on power laws for flow resistance. J Hydraulic Eng – ASCE 1991;117(3):371–89.
[39] Katul GG, Wiberg P, Albertson J, Hornberger G. A mixing layer theory for flow resistance in shallow streams. Water Resour Res 2002;38(11).
[40] Katul G, Poggi D, Ridolfi L. A flow resistance model for assessing the impact of vegetation on flood routing mechanics. Water Resour Res., in press.
[41] Bureau of Meteorology. Intensity frequency duration curves for Karratha, Western Australia; 2009.
[42] Galle S, Ehrmann M, Peugeot C. Water balance in a banded vegetation pattern – a case study of tiger bush in western Niger. Catena 1999;37(1–2):197–216.
[43] Bureau of Meteorology. Rainfall statistics for Menindee, NSW; 2011.
[44] Dunkerley D, Brown KJ. Oblique vegetation banding in the australian arid zone: implications for theories of pattern evolution and maintenance. J Arid Environ 2002;51:163–81.
[45] Thompson SE, Katul GG, MacMahon S. Role of biomass spread in vegetation pattern formation within arid ecosystems. Water Resour Res 2008;44(E10421).